J. Fluid Mech. (2000), *vol.* 403, *pp.* 263–276. Printed in the United Kingdom

Experimental investigation of dynamo effect in the secondary pumps of the fast breeder reactor Superphenix

By A. ALEMANY, Ph. MARTY, F. PLUNIAN AND J. SOTO

Laboratoire LEGI, BP 53 X, F-38041 Grenoble cedex, France

(Received 31 July 1998 and in revised form 9 September 1999)

The fast breeder reactors (FBR) BN600 (Russia) and Phenix (France) have been the subject of several experimental studies aimed at the observation of dynamo action. Though no dynamo effect has been identified, the possibility was raised for the FBR Superphenix (France) which has an electric power twice that of BN600 and five times larger than Phenix. We present the results of a series of experimental investigations on the secondary pumps of Superphenix. The helical sodium flow inside one pump corresponds to a maximum magnetic Reynolds number (R_m) of 25 in the experimental conditions (low temperature). The magnetic field was recorded in the vicinity of the pumps and no dynamo action has been identified. An estimate of the critical flow rate necessary to reach dynamo action has been found, showing that the pumps are far from producing dynamo action. The magnetic energy spectrum was also recorded and analysed. It is of the form $k^{-11/3}$, suggesting the existence of a large-scale magnetic field. Following Moffatt (1978), this spectrum slope is also justified by a phenomenological approach.

1. Introduction

1.1. *Magnetic Reynolds numbers in FBRs*

The coolant used in a fast breeder reactor (FBR) is liquid sodium, chosen essentially for its high thermal conductivity and its weak absorption of neutron flux. The liquid sodium is also characterized by a strong electrical conductivity which, coupled with a sufficiently high flow rate, can yield a large magnetic Reynolds number R_m defined by

$$R_m = \mu\sigma UL, \tag{1.1}$$

where σ and μ are the electrical conductivity and magnetic permeability of the sodium, L and U some relevant length scale and intensity of its motion. Bevir (1973) and M. Steenbeck (1973, personal communication from K.-H. Rädler) first pointed out the possibility for dynamo action to take place in an FBR due to the large values of R_m. Estimates of R_m under working conditions and for different relevant zones of the FBR BN600, Phenix and Superphenix are given in table 1. These values are indeed much larger than unity. However the geometry of the sodium flow may not be necessarily appropriate for dynamo action. In particular, a weak helicity would make the occurrence of dynamo action difficult. Therefore, a qualitative evaluation of the helicity is also given in table 1 for the different zones of the FBR. The locations of these zones are sketched in figure 1. The location of the magnetometers and coils of previous experiments are also indicated.

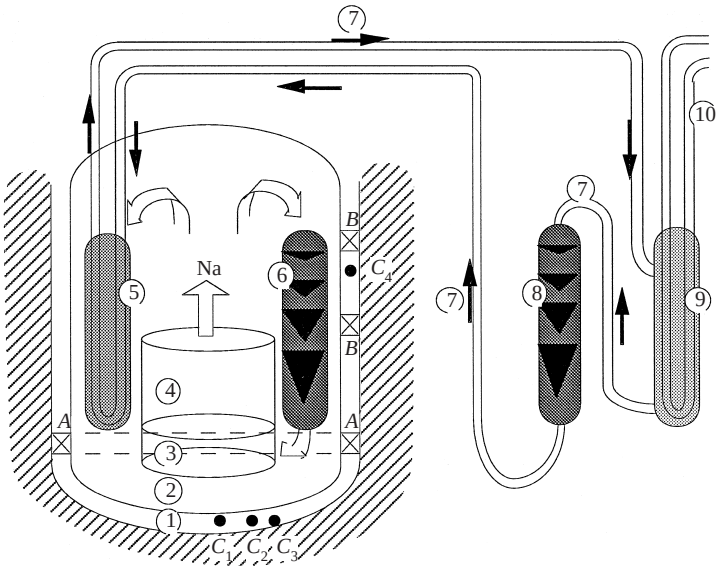

FIGURE 1. Schematic of an FBR: 1. inter tank, 2. tank containing the primary sodium (diameter of 20 m), 3. pressure chamber, 4. core (diameter of 6 m), 5. primary-secondary heat exchanger, 6. primary pump, 7. secondary loop of sodium, 8. secondary pump, 9. secondary-water heat exchanger, 10. water loop. The white (black) arrows show the sodium motion in the primary (secondary) loop. Two coils (AA' and BB') and four magnetometers (C_1, C_2, C_3, C_4) were set up in the FBR BN600.

		Pressure chamber	Core	Primary pump	Secondary pump	Heat exchanger
Helicity		mean	strong	mean	mean	weak
	BN600	17	18	13	no info	no info
R_m	Phenix	15	13	8	7	no info
	Superphenix	30	30	15	16	8

TABLE 1. Qualitative estimate of helicity and magnetic Reynolds number for relevant zones of the FBRs BN600, Phenix and Superphenix. The conductivity corresponds to the mean temperature under working conditions. Its value is $\sigma = 5 \times 10^6\ \Omega^{-1}\,\mathrm{m}^{-1}$ at 400 °C (Freedman & Robertson 1961). For the secondary pumps of Superphenix, the characteristic length and velocity of the outflow are 0.5 m and $5\,\mathrm{m\,s}^{-1}$, leading to $R_m = 16$.

1.2. *Previous studies on FBRs*

The previous experiments in FBRs concerned mainly the pressure chamber, one primary pump of BN600, and one secondary pump of Phenix. The vicinity of the pressure chamber of BN600 has been investigated by Kirko, Mitenkov & Barannikov (1981). Three magnetic probes were located under the pressure chamber along an axis of delivery of one of the primary pumps (figure 1). An external vertical magnetic field could be externally applied by an electric current in a coil encircling the tank containing the primary sodium (AA'). A vertical large-scale field has been measured. It was enhanced by either increasing the velocity of the pumps or increasing the thermal power of the reactor. To explain these observations, Kirko (1984) suggests the existence of thermoelectric currents coupled with an α^2-effect in the pressure chamber due to the asymmetrical disposition of the pumps. The critical regime above

which self-excitation would happen has been estimated in terms of the reactor power. The designed working conditions of BN600 and Superphenix have been found to be subcritical by respectively Kirko (1989) and Garnier (1986).

Magnetic measurements in the vicinity of one primary pump of BN600 (C_4 in figure 1) have revealed the existence of thermoelectric currents. For a given power of the pumps, a correlation between the magnetic field intensity and the thermal power of the reactor has been detected (Kirko *et al.* 1982*a*). Moreover, magnetic fluctuations correlated with the pump input power and the thermal input power have been observed (Kirko *et al.* 1982*b*). Kirko (1989) suggests that their origin may be in the existence of Alfvén waves, due to an azimuthal magnetic field generated in the pressure chamber.

One secondary pump of Phenix was investigated by Werkoff & Garnier (1988). A transverse magnetic field was externally applied with Helmholtz coils located at the pump outlet. With potential probes in contact with the outflow pipe, a deformation of the magnetic field by the axial sodium motion in the pump was measured. No magnetic self-excitation was identified.

Other studies on the FBR have been undertaken, either related to the existence of thermoelectric currents (Gailitis & Freiberg 1992; Marty, Ajakh & Thess 1994) or dynamo action in the core (Plunian, Marty & Alemany 1999).

1.3. *Motivation*

The reactor Superphenix seems to be a better candidate for dynamo action than BN600 and Phenix because of its larger dimensions. We investigated its four secondary pumps (denoted pumps 1 to 4) for they are a good compromise between scientific interest and experimental accessibility. The possibility of additional head losses due to dynamo action in the secondary pumps of Superphenix was the subject of controversy before the first run of the reactor. Ten years later, this paper brings an experimental answer to this question. We also investigated the characteristics of the MHD turbulence produced by the sodium flow and compared the experimental results with theoretical predictions.

2. Experimental conditions

2.1. *The sodium flow*

Each pump is axisymmetric around its vertical axis (figure 2). The mean sodium flow is almost purely azimuthal near the rotor, the resulting helicity being close to zero. Then it is straightened by fixed helical foils in its way down, in order that the flow is almost purely axial at the exit, the resulting helicity being also close to zero. However, between the rotor and the exit, the helicity is non-zero and reaches a maximum. This helical flow is surrounded by the incoming sodium flow which is roughly axial and directed upwards. The outer region of the pump is filled with sodium with a slow motion compared to the inner velocity.

During the experiments, the sodium temperature was kept as low as possible (200 °C), in order to ensure the highest electrical conductivity possible. The velocity Ω of each pump could vary from 110 to 492 r.p.m., the minimum value of 110 r.p.m. being necessary to ensure a thermal flux high enough to prevent the sodium from solidifying. At a temperature of $T = 200\,^{\circ}\mathrm{C}$, for which $\sigma_{Na} = 7.8 \times 10^6\,\Omega^{-1}\,\mathrm{m}^{-1}$, and for a pump velocity $\Omega = 492$ r.p.m. corresponding to an outflow velocity of $5\,\mathrm{m\,s}^{-1}$, the outflow radius being of 0.5 m, an estimate of R_m is 25.

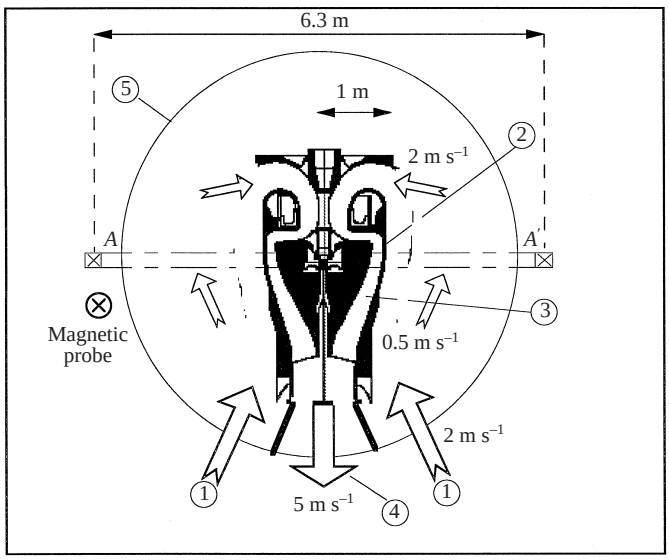

FIGURE 2. Vertical cross-section of a secondary pump showing also the location of the magnetic probes and external copper coil (AA') used in the experiments on Superphenix. 1. Sodium inflow, 2. region of maximum flow rotation driven by rotating blades, 3. flow straightening by static helical foils, 4. sodium outflow directed downwards and without rotation, 5. housing containing sodium with slow motion.

2.2. *External coil*

A copper coil (diameter 6.3 m × section 25 mm^2) was wound around pumps 3 and 4 (40 turns) in order to generate an external magnetic field in the pump. The idea is to measure the magnetic decay time after the current in the coil is suddenly switched off, an infinite decay time corresponding to dynamo action. This technique has already been used by various authors (e.g. Gailitis *et al.* 1989; Joussellin *et al.* 1989). Figure 3 shows the electrical arrangement. A DC power supply provides an electric current adjustable up to 30 A in the coil. It produces a maximum field intensity of 2.5 G, approximately eight times the Earth's field. A diode is also connected to avoid any electric arc when the circuit breaker is switched off. We note that in absence of a coil (pumps 1 and 2) or a current in the coil (pumps 3 and 4), the applied field $\boldsymbol{B}_0$ is not only the Earth's field but in addition the field coming from the industrial environment. As a result, $\boldsymbol{B}_0$ varied from one pump to another.

2.3. *Magnetic measurements*

The magnetic measurements were performed at the vicinity of each pump, with a flux gate magnetometer. This probe measures simultaneously the three components and the modulus of the magnetic field with an accuracy of 10^{-9} T. Each component and the modulus was recorded on a separate channel. The signals were recorded with a magnetic recorder (TEAC RD 135 T) with a sampling frequency of 24 kHz.

Let us introduce the notation which is used in the rest of the paper. The field which is measured is denoted $\boldsymbol{B}_{total}$. The mean and fluctuating parts of $\boldsymbol{B}_{total}$ are denoted $\boldsymbol{B}$ and $\boldsymbol{b}$. They satisfy

$$\boldsymbol{B}_{total} = \boldsymbol{B} + \boldsymbol{b}, \quad \text{with} \quad \boldsymbol{B} = \langle \boldsymbol{B}_{total} \rangle \quad \text{and} \quad \langle \boldsymbol{b} \rangle = \boldsymbol{0} \tag{2.1}$$

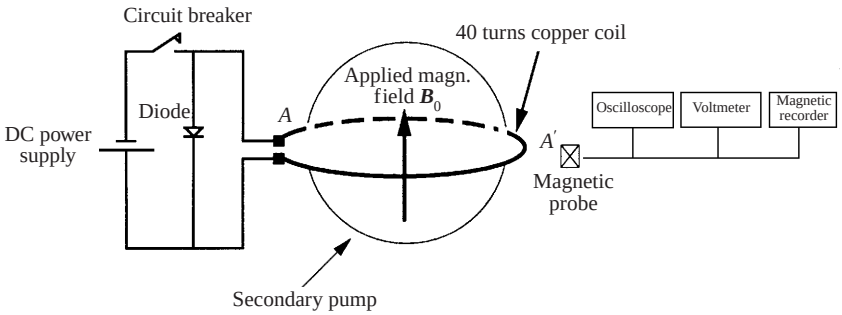

FIGURE 3. Electrical arrangement for pumps 3 and 4 (this coil is shown as AA' in figure 2). After the power supply has been disconnected, the current flows through the diode for approximately 0.12 s (see figure 6).

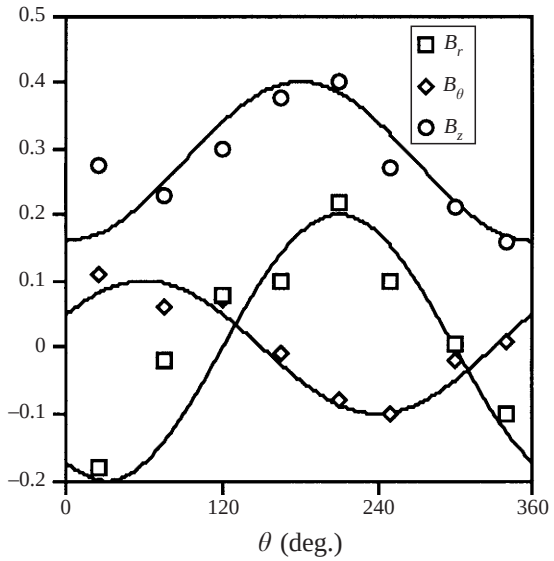

FIGURE 4. Azimuthal dependence of B_r, B_θ and B_z (in G) for $\Omega = 350$ r.p.m. The data points are the experimental measurements made on pump 1. The curves are obtained from a sinusoidal fit.

where $\langle\ \rangle$ denotes a time average. Attention is successively confined to the analysis of the mean field $\boldsymbol{B}$ (§ 3) and of the fluctuating field $\boldsymbol{b}$ (§ 4).

3. The mean field

3.1. *Geometry of the mean field*

The azimuthal dependence of $\boldsymbol{B}$ has been measured at the vicinity of pump 1 for $\Omega = 350$ r.p.m. and without a coil around the pump. In figure 4, the cylindrical components B_r, B_θ and B_z are plotted versus θ. The measurements can be approximated by the following fit corresponding to the curves in figure 4:

$$B_r = -0.2\cos(\theta - \tfrac{1}{6}\pi), \quad B_\theta = 0.1\cos(\theta - \tfrac{1}{3}\pi), \quad B_z = 0.28 - 0.12\cos(\theta). \tag{3.1}$$

It is straightforward to show from (3.1) that $\boldsymbol{B}$ is the sum of a constant field $\boldsymbol{B}_0$ plus an additional field $\boldsymbol{B}_1$ characterized by an azimuthal mode $m = 1$. This is consistent

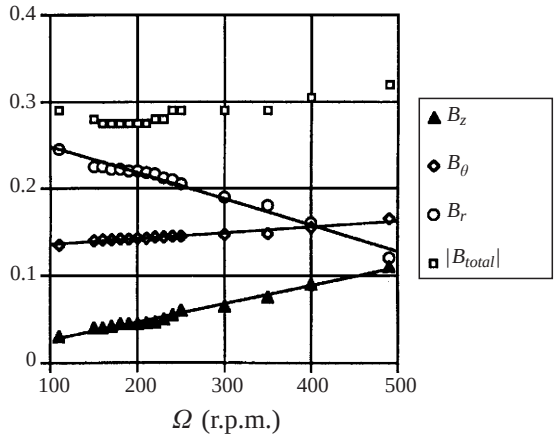

FIGURE 5. The mean field components B_r, B_θ, B_z (in G) and the modulus of the total field $|B_{total}|$ versus the velocity of pump 2.

with previous theoretical findings about rotating flows (see e.g. Moffatt 1978), $\boldsymbol{B}_1$ coming from the distortion of $\boldsymbol{B}_0$ by the differential rotation of the flow.

Figure 5 shows $\boldsymbol{B}$ measured in the vicinity of pump 2 for different velocities and without a coil around the pump. One can see a clear decrease of B_r and a slight increase of B_θ and B_z when the velocity is increased. Again, this behaviour can be interpreted in terms of distortion of the field by the inner helical motion. Indeed, it is clear that the distortion is stronger for higher velocities, the resulting field tending to be also helical.

The differential rotation may be an important mechanism of dynamo action. Furthermore it is well known that when the flow is axisymmetric, the mode $m = 1$ is generally the most unstable one (see e.g. Gailitis *et al.* 1989). As a result, the magnetic field already has a geometry appropriate for dynamo action. Then, it is likely that dynamo action would occur for a higher velocity (see § 3.2).

In figure 5, the modulus of the total field $|\boldsymbol{B}_{total}|$ is also plotted versus the pump velocity. The fluctuating part $\boldsymbol{b}$, though it has a zero time average also contributes to $|\boldsymbol{B}_{total}|$ through $|\boldsymbol{B}_{total}| = \left(\boldsymbol{B}^2 + \langle \boldsymbol{b}^2 \rangle\right)^{1/2}$. The modulus of the mean field $|\boldsymbol{B}| = \left(B_r^2 + B_\theta^2 + B_z^2\right)^{1/2}$ can be deduced from the other curves of figure 5. It slightly decreases versus Ω whereas $|\boldsymbol{B}_{total}|$ increases versus Ω. The difference comes from the intensification of the turbulence for increasing velocity, as it will be explained in § 4.

3.2. *Estimate of the critical R_m of the pump*

In this subsection, an additional field is imposed by the external coil described in § 2.2 around pump 3. A typical plot of B_θ versus time is given in figure 6. The curve presents three zones corresponding first to an initial steady state (with a current in the coil), second to a steep magnetic decay (after the current has been switched off) and third to the diffusion of the magnetic field (after $t_0 \approx 40$ s). This last period does not represent the most suitable basis for the analysis of a possible self-excitation. Indeed, the decrease or increase of the most unstable mode can only be identified after the decay of all the other modes of the mode mixture resulting from the applied magnetic field. The decay time t_d of those modes, for a sphere of radius R is in the

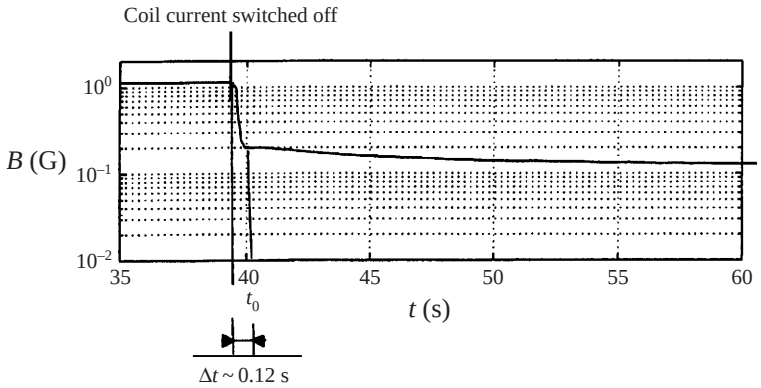

FIGURE 6. Typical time evolution of B_θ in the vicinity of pump 3. After the current is switched off in the copper coil, the ohmic decay of the electrical current in the coil lasts about 0.12 s.

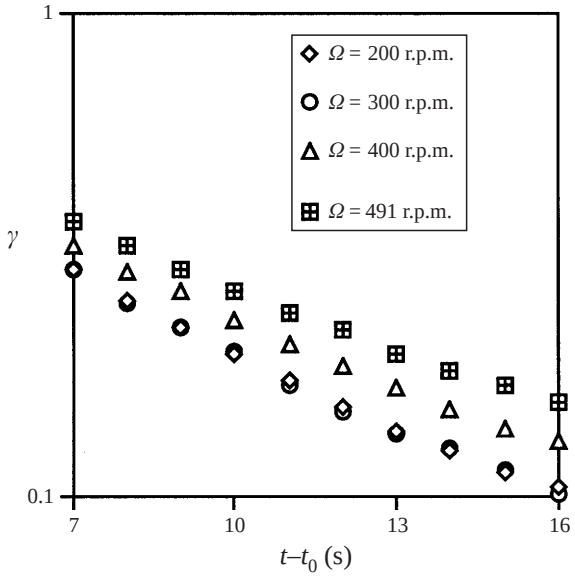

FIGURE 7. Logarithmic plot of γ versus $(t-t_0)$, γ being defined in equation (3.3). The different curves correspond to different values of Ω. The time t_0 corresponds to the end of the steep decay of the current in the copper coil. Only the period of time starting at $t - t_0 = 7$ s is shown as it is the basis of the dynamo analysis.

order of

$$t_d \approx \frac{\sigma \mu R^2}{\pi^2}, \tag{3.2}$$

leading to $t_d = 6.2$ s for $R = 2.5$ m and $\sigma_{Na} = 7.8 \times 10^6\,\Omega^{-1}\,\mathrm{m}^{-1}$. Therefore, only the time signal starting at $t_0 + t_d \approx 47$ s is of relevance for the analysis of dynamo action. The ratio γ versus $(t-t_0)$ is plotted in figure 7 for different values of Ω, with γ defined by

$$\gamma = \frac{B_\theta(t) - B_\theta(t_\infty)}{B_\theta(t_0 + t_d) - B_\theta(t_\infty)}, \tag{3.3}$$

Ω (r.p.m.)	200	300	400	491
p (s^{-1})	−0.117	−0.117	−0.106	−0.0987

TABLE 2. The growth rate p versus the pump velocity.

the asymptotic value of B_θ being $B_\theta(t_\infty) \approx 0.15\,\mathrm{G}$. A time dependence of the form $B_\theta(t) = B_\theta(t_\infty) + (B_\theta(t_0 + t_d) - B_\theta(t_\infty))\mathrm{e}^{pt}$ can be deduced from figure 7, considering only the period of time starting at $t - t_0 = 7\,\mathrm{s}$. The growth rate p, though always negative, is found to increase with Ω, suggesting that dynamo action ($p = 0$) may be reached for a sufficiently high flow rate. The values of p versus Ω are given in table 2. Extrapolating linearly those values to $p = 0$ leads to a critical pump velocity of 2000 r.p.m. corresponding to four times the maximum regime of a secondary pump of Superphenix, i.e. $R_m = 100$. This last result is of very speculative character because of the small amount of data. However, the main conclusion is that the secondary pumps of Superphenix are far from producing dynamo action.

4. Turbulence analysis

4.1. *Theoretical analysis*

Attention is now turned not only to the mean magnetic field $\boldsymbol{B}$ but also to the magnetic fluctuation $\boldsymbol{b}$, the total magnetic field being defined by (2.1). The sodium velocity is also defined by $\boldsymbol{U} + \boldsymbol{u}$, where $\boldsymbol{U}$ is the mean part and $\boldsymbol{u}$ the fluctuating part. We denote l_0 the integral scale of the turbulent motion and u_0 the corresponding turbulent flow intensity. The turbulent motion of this experimental situation is thus characterized by a turbulent magnetic Reynolds number R_{mt} defined by

$$R_{mt} = \frac{u_0 l_0}{\lambda}. \tag{4.1}$$

For $T = 200\,^\circ\mathrm{C}$ ($\sigma_{Na} = 7.8 \times 10^6\,\Omega^{-1}\,\mathrm{m}^{-1}$) and assuming that u_0 and l_0 are respectively about 10% of the typical mean velocity ($U_0 = 0.5\,\mathrm{m\,s}^{-1}$ in the outer region of the pump) and 10% of the container radius (2.5 m), we obtain

$$R_{mt} \approx 0.1.$$

Under such conditions the turbulence is characterized only by the interaction parameter N which is defined as the ratio of the eddy turnover time l_0/u_0 (which characterizes the inertia) to the Joule dissipation time $\rho/\sigma B^2$:

$$N = \frac{B^2 \sigma l_0}{\rho u_0}. \tag{4.2}$$

In the presence of a strong external magnetic field, N is large and the turbulent flow is then dominated by the electromagnetic forces, the energy being mainly dissipated by the Joule effect. In that case, and when R_{mt} is low, the flow may have a quasi-two-dimensional structure and the kinetic energy spectrum is of the form k^{-3} (Alemany *et al.* 1979; Sommeria & Moreau 1982; Caperan & Alemany 1985). On the other hand, when the interaction parameter is smaller than unity, which is the case in the present study where

$$N \approx 10^{-4},$$

the turbulence is controlled by the inertia forces. The corresponding picture of the turbulent flow is then conventional, with an inertial and a dissipative range. In that case the kinetic energy spectrum is of the form

$$E(k) = O(k^{-5/3}). \tag{4.3}$$

Now, following Moffatt (1978), the induction equation may be separated into its mean and fluctuating parts. A legitimate approximation of the latter, in the case of conventional turbulence and small R_{mt}, is

$$0 = \nabla \times (\boldsymbol{u} \times \boldsymbol{B}) + \lambda \nabla^2 \boldsymbol{b}. \tag{4.4}$$

This equation states that the magnetic fluctuations $\boldsymbol{b}$ are generated by the interaction of $\boldsymbol{u}$ with the local mean field $\boldsymbol{B}$. From (4.4), the relation between the Fourier transforms of the second-order correlations of $\boldsymbol{u}$ (denoted $\hat{u}_{ij}$) and $\boldsymbol{b}$ (denoted $\hat{b}_{ij}$) can be derived

$$\hat{b}_{ij} = -\frac{1}{k^2} \frac{B^2 \cos^2 \theta}{\lambda^2} \hat{u}_{ij}, \tag{4.5}$$

where θ represents the angle between the wave vector $\boldsymbol{k}$ and $\boldsymbol{B}$. Assuming that the turbulence is isotropic, we can integrate these second-order correlations on a sphere of radius k in the wave vector space (Lahjomri 1988). It yields the following relation between the magnetic energy spectra $E_m(k)$ and the kinetic energy spectra $E(k)$:

$$E_m(k) \approx E(k) k^{-2}. \tag{4.6}$$

From (4.3), the magnetic energy spectrum then takes the form

$$E_m(k) = O(k^{-11/3}). \tag{4.7}$$

It is clear, by comparing the two spectra (4.3) and (4.7), that the integral scale of the magnetic energy distribution is larger than that of the kinetic energy.

4.2. *Influence of the probe location*

Before analysing the magnetic spectra that we obtained, we first give an estimate of the range of frequencies for which our measurements are relevant. With a probe located outside the pump container, the signal of too high frequencies coming from the inner part will be filtered out. On the other hand, the size of the largest magnetic structures which exist inside the container yield a lower bound for the range of relevant frequencies. In order to evaluate the highest relevant frequency, we use the law of Biot and Savart

$$\boldsymbol{b} = \frac{1}{4\pi} \int_V \frac{\mu \boldsymbol{j} \times \boldsymbol{r}}{r^3} \, \mathrm{d}V, \tag{4.8}$$

where $\boldsymbol{b}$ is the magnetic signal at the probe, $\boldsymbol{j}$ the turbulent current density inside the control volume V and $\boldsymbol{r}$ the relative position vector between the local current density and the magnetic probe. Assuming a homogeneous repartition of $\boldsymbol{j}$ in the liquid sodium, $\boldsymbol{j}$ can be written in the form of a Fourier integral expansion

$$\boldsymbol{j}(\boldsymbol{r}, t) = \int_{-\infty}^{\infty} \mathrm{e}^{2\mathrm{i}\pi(\boldsymbol{k}\cdot\boldsymbol{x})} \hat{\boldsymbol{j}}(\boldsymbol{k}, t) d^3\boldsymbol{k}, \tag{4.9}$$

where the Fourier transform $\hat{\boldsymbol{j}}(\boldsymbol{k}, t)$ depends on the wave vector $\boldsymbol{k}$. In the Cartesian frame $(\boldsymbol{e}_x, \boldsymbol{e}_y, \boldsymbol{e}_z)$ defined in figure 8, the vector position $\boldsymbol{x}(x, y, z)$ is defined by $\boldsymbol{x} = \boldsymbol{r} - \boldsymbol{x}_0$ where $\boldsymbol{x}_0(x_0, 0, 0)$ is the position vector between the probe and the wall of the container.

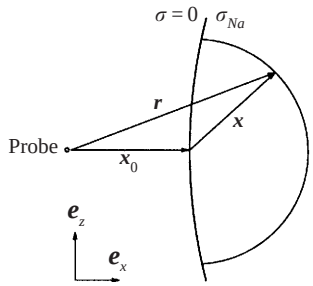

FIGURE 8. Fluid domain in which magnetic frequencies lower than U_0/x_0 are significantly detected by the probe.

From (4.8) and (4.9), $\boldsymbol{b}$ can be written

$$\boldsymbol{b} = \frac{\mu}{4\pi} \int_{\boldsymbol{k}} \hat{\boldsymbol{j}}(\boldsymbol{k}, t) \times \left(\int_V \mathrm{e}^{2\mathrm{i}\pi(\boldsymbol{k}\cdot\boldsymbol{x})} \frac{\boldsymbol{r}}{|r|^3} \, \mathrm{d}V \right) \mathrm{d}^3\boldsymbol{k}. \tag{4.10}$$

Replacing $|r|$ by its expression in terms of x, y, z and x_0, (4.10) becomes

$$\boldsymbol{b} = \frac{\mu}{4\pi {x_0}^2} \int_{\boldsymbol{k}} \hat{\boldsymbol{j}}(\boldsymbol{k}, t) \times \left(\int_V \mathrm{e}^{2\mathrm{i}\pi\boldsymbol{k}\cdot\boldsymbol{x}} \boldsymbol{F} \, \mathrm{d}V \right) \mathrm{d}^3\boldsymbol{k}, \tag{4.11}$$

where $\boldsymbol{F}$ is a convolution kernel defined by

$$\boldsymbol{F} = \frac{(1 + x/x_0)\boldsymbol{e}_x + (y/x_0)\boldsymbol{e}_y + (z/x_0)\boldsymbol{e}_z}{\left((1 + x/x_0)^2 + (y/x_0)^2 + (z/x_0)^2\right)^{3/2}}. \tag{4.12}$$

Each component of $\int_V \boldsymbol{F} \, \mathrm{d}V$ converges and has a typical radius of convergence of the order of x_0. Therefore, we can approximate (4.11) by

$$\boldsymbol{b} = \frac{\mu}{4\pi {x_0}^2} \int_{|\boldsymbol{k}| \leqslant |\boldsymbol{k}_0|} \hat{\boldsymbol{j}}(\boldsymbol{k}, t) \times \mathrm{e}^{2\mathrm{i}\pi\boldsymbol{k}\cdot\boldsymbol{x}} \left(\int_V \boldsymbol{F} \, \mathrm{d}V \right) \mathrm{d}^3\boldsymbol{k} + \frac{\mu}{4\pi {x_0}^2} \int_{|\boldsymbol{k}| > |\boldsymbol{k}_0|} \hat{\boldsymbol{j}}(\boldsymbol{k}, t) \times \left(\int_V \mathrm{e}^{2\mathrm{i}\pi\boldsymbol{k}\cdot\boldsymbol{x}} \boldsymbol{F} \, \mathrm{d}V \right) \mathrm{d}^3\boldsymbol{k}, \tag{4.13}$$

where $|k_0| \approx 1/x_0$. This means that there is a range of frequencies ($|\boldsymbol{k}| \leqslant |\boldsymbol{k}_0|$) for which the spectrum of $\boldsymbol{b}$ has the same slope as the spectrum of $\boldsymbol{j}$. Therefore, this range of frequencies is relevant to the magnetic fluctuations in the liquid sodium. It also shows that the closer to the wall the probe is, the larger this relevant spectrum is. The frequency corresponding to an eddy of typical wavenumber $\boldsymbol{k}$ can be derived under the assumption of ergodicity leading to $f = |k|U_0$, where, again, U_0 is a typical value of the mean velocity in the control volume. This yields a higher bound:

$$f_{max} = U_0/x_0. \tag{4.14}$$

In our experiment, $x_0 \approx 0.5\,\mathrm{m}$ and $U_0 = 0.5\,\mathrm{m\,s^{-1}}$, leading to $f_{max} = 1\,\mathrm{Hz}$. Higher frequencies $f > f_{max}$ are also seen by the probe but they are not self-similar anymore, i.e. their filtering depends not only on the location of the perturbation but also on their phase shift. Therefore, they are not relevant.

The lowest relevant frequency is evaluated on the basis of the turnover time of the largest possible structures

$$f_{min} = U_0/L, \tag{4.15}$$

where L is the size of the device. For $L = 5\,\mathrm{m}$, (4.15) leads to $f_{min} = 0.1\,\mathrm{Hz}$.

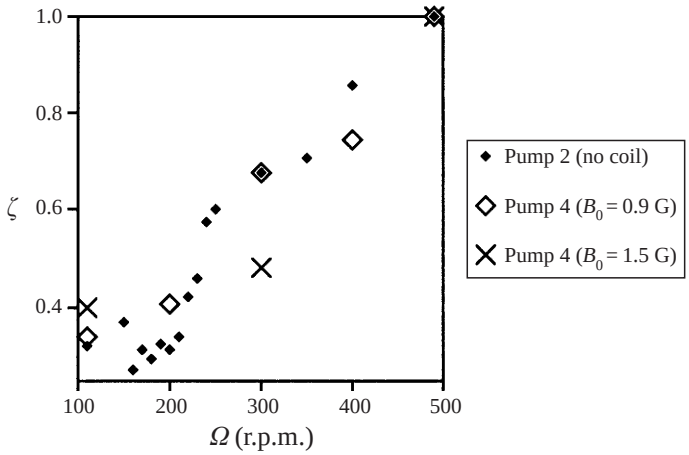

FIGURE 9. The dimensionless magnetic turbulence intensity ζ versus the angular velocity Ω for different pumps and different values of the applied magnetic field B_0.

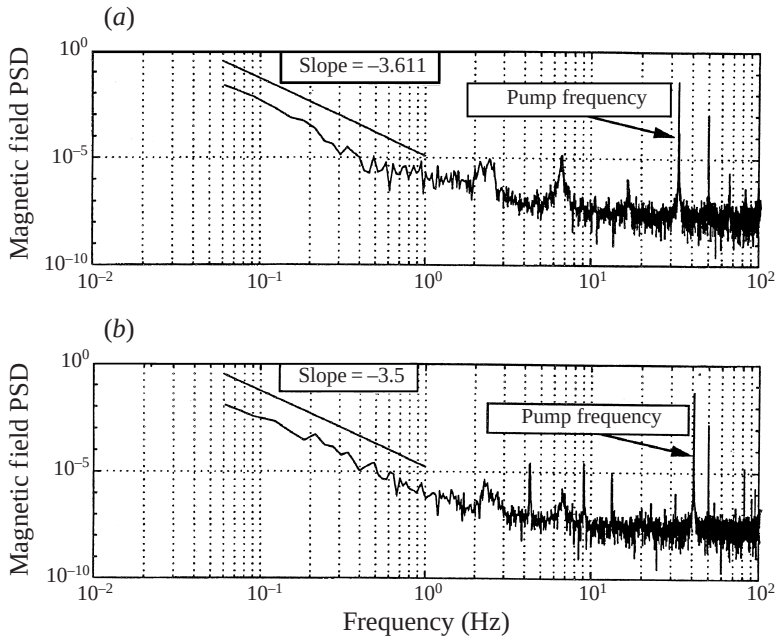

FIGURE 10. Magnetic power spectral density (PSD) when the velocity of pump 4 is 400 r.p.m. (*a*) and 492 r.p.m (*b*). A magnetic field of 2 G is externally applied in addition to the Earth's field.

4.3. *Experimental results*

The magnetic signal has been recorded for the same range of velocities as in § 3, but on pump 4 and both without and with an externally applied field. A maximum of 2 min of signal was recorded. Therefore, only the frequencies larger than 5×10^{-2} Hz were measured which is enough to cover the range of relevant frequencies [0.1 Hz; 1 Hz] which has been derived in § 4.2. The spectrum of the magnetic power density was calculated with the Welch (1970) method. The results are presented in figures 9, 10 and 11.

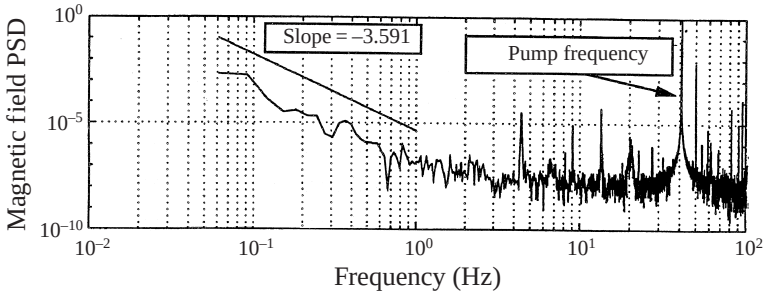

FIGURE 11. Same as figure 10(*b*) but without externally applied field (only the Earth's field is present).

In figure 9 the dimensionless magnetic turbulence intensity $\zeta(\Omega)$ is plotted versus the pump velocity Ω, with

$$\zeta(\Omega) = \frac{\langle \boldsymbol{b}^2(\Omega)\rangle^{1/2}}{\langle \boldsymbol{b}^2(\Omega_{max})\rangle^{1/2}} \quad \text{and} \quad \Omega_{max} = 492\,\text{r.p.m.} \tag{4.16}$$

These results are given in a dimensionless form in order to compare the data obtained for different pumps and different externally applied magnetic fields. The curve corresponding to pump 2 is directly derived from the data of figure 5, applying the relation $\langle \boldsymbol{b}\rangle^{1/2} = \left(\boldsymbol{B}^2_{total} - \boldsymbol{B}^2\right)^{1/2}$.

As R_{mt} is much smaller than unity, it is reasonable to assume that $\langle \boldsymbol{b}^2\rangle^{1/2} = O(R_{mt})$. Furthermore, we can also assume that $R_{mt} = O(\Omega)$. Therefore, a linear increase of the turbulent magnetic intensity with the pump velocity is expected. This tendency is indeed confirmed by the results of figure 9.

Concerning the magnetic energy spectrum, the most significant results have been obtained for the highest values of Ω. The spectra for $\Omega = 400$ and 492 r.p.m. and an applied field of intensity $B_0 = 2\,\text{G}$ are shown in figure 10. Each spectrum presents two typical zones. The high frequency zone (1–100 Hz) corresponds to the noise of the magnetic environment of the pump. In particular, the magnetic signature of the rotation of the pump itself plus the harmonics of its fundamental frequency can be precisely identified. The low frequency zone (5×10^{-2}–1 Hz) corresponds to the magnetic fluctuations inside the sodium flow. In this zone, the slope of the spectrum is equal to -3.6 in one case and -3.5 in the other case. These values correspond quite well with the theoretical value $-\frac{11}{3}$ predicted in § 4.1 for an isotropic turbulence. A slope around -3.6 is also obtained for $\Omega = 492$ r.p.m. and without current in the external coil (figure 11).

5. Conclusion

This paper presents the results of magnetic recordings in the vicinity of the four secondary pumps of the FBR Superphenix.

Our first motivation was to see whether dynamo action could take place in a pump which has a magnetic Reynolds number larger than unity and a non-zero helicity. Though no dynamo action has been identified, we can reasonably expect that a stronger flow rate would produce a self-excitation. Indeed, if the Earth's field (or any externally applied field) is subtracted from the mean field, then the remaining field has an azimuthal mode $m = 1$ as expected to be produced by an axisymmetric

helical flow. To reach the dynamo threshold, the extrapolation of our experimental results leads to a pump velocity of 2000 r.p.m. corresponding to a critical magnetic Reynolds number of 100. The maximum possible pump velocity is actually 492 r.p.m. and therefore far from producing dynamo action.

We have also quantified the magnetic turbulence resulting from the interaction of the flow fluctuations and the mean field. The best results were found when applying an external field to the pump with a copper coil wound around the pump. The results were interpreted with an appropriate analysis based on orders of magnitude. In particular, the finding of a magnetic spectrum in $k^{-11/3}$ is consistent with the low values of the turbulent magnetic Reynolds number and interaction parameter. This analysis is also consistent with the linear dependency of the magnetic turbulence intensity with the pump velocity.

We are very grateful to the Direction of Superphenix for allowing us to make our measurements and to the reactor Staff for financial and technical support. We also thank the Direction of Electricité de France and particularly the Centre Lyonnais d'Ingénierie for its help in obtaining access to Superphenix. Some experimental equipment has been provided by the Groupement de Recherche de Mécanique des Fluides Géophysiques et Astrophysiques which is acknowledged. We also gratefully acknowledge the referees for helpful comments.

REFERENCES

Alemany, A., Moreau, R., Sulem, P. L. & Frisch, U. 1979 Influence of an external magnetic field on homogeneous MHD turbulence. *J. Méc.* **18**, 273–313.

Bevir, M. K. 1973 Possibility of electromagnetic self-excitation in liquid metal flows in fast reactors. *J. Brit. Nucl. Engng Soc.* **12**, 455–458.

Caperan, P. & Alemany, A. 1985 Turbulence homogène MHD à faible nombre de Reynolds magnétique. Etude de la transition vers la phase quasi bidimensionnelle et caractérisation de son anisotropie. *J. Méc. Théor. Appl.* **4**, 175–200.

Freedman, J. F. & Robertson, W. D. 1961 Electrical resistivity of liquid sodium, liquid lithium and dilute liquid sodium solutions. *J. Chem. Phys.* **34**, 769–780.

Gailitis, A. & Freiberg, Ya. 1992 Magnetic Field due to thermoelectric currents in a fast reactor. *Magnetohydrodynamics* **4**, 96–100.

Gailitis, A., Lielausis, O., Karasev, B. G., Kirillov, I. R. & Ogorodnikov, A. P. 1989 The helical MHD dynamo. In *Liquid Metal Magnetohydrodynamics* (ed. J. Lielpeteris & R. Moreau), pp. 413–419. Kluwer.

Garnier, J. 1986 Synthèse et critique des travaux de l'Académie des Sciences Soviétique concernant les effets thermoélectromagnétohydrodynamiques dans les surgénérateurs. *CEA Tech. Rep.* (STT/LTMP/86-07-C/JG).

Garnier, J. & Werkoff, F. 1987 Some of the MHD effects in liquid-metal fast breeder reactors. *Prog. Astronaut. Aeronaut.* **111**, 339–348.

Joussellin, F., Marty, P., Alemany, A. & Werkoff, F. 1989 MHD induction generator at low magnetic Reynolds number: Part II – numerical modelling and experimental study. *Eur. J. Mech.* **8**, n.4.

Kirko, G. E. 1984 Phénomènes électromagnétiques dans les grandes masses de métaux liquides. trad. CEA N 2.722.1.

Kirko, G. E. 1989 MHD phenomena in fast neutron reactors with a liquid metal heat carrier. In *Liquid Metal Magnetohydrodynamics* (ed. J. Lielpeteris & R. Moreau), pp. 425–429. Kluwer.

Kirko, I. M., Kirko, G. E., Sheinkman, A. G. & Telichko, M. T. 1982 On the existence of thermoelectric currents in the BN-600 reactor of the Beloyarsk atomic power plant. *Dokl. Akad. Nauk. SSSR* **266**, 854 [English transl. *Sov. Phys. Dokl.* **27**, 873].

Kirko, I. M., Kirko, G. E., Telichko, M. T. & Sheinkman, A. G. 1982 Experimental detection of

the generation of a magnetic field liquid metal for magnetic Reynolds number much larger than unity. *Dokl. Akad. Nauk. SSSR* **266**, 854 [English transl. *Sov. Phys. Dokl.* **27**, 10].

Kirko, I. M., Mitenkov, F. M. & Barannikov, V. A. 1981 Observation of MHD phenomena in liquid metal of the primary loop of a BN-600 fast reactor at the Beloyarsk nuclear power plant. *Dokl. Akad. Nauk. SSSR* **257**, 861–863 [English transl. *Sov. Phys. Dokl.* **26**, 427].

Lahjomri, J. 1988 Caractérisation de la structure des sillages MHD amont et aval d'un cylindre à petit nombre de Reynolds magnétique. PhD thesis, Joseph Fourier University, Grenoble.

Marty, P., Ajakh, A. & Thess, A. 1994 Magnetic fields in fast breeder reactors: new results on thermoelectricity and dynamo effect. *Magnetohydrodynamics* **30**, 474–485.

Moffatt, H. K. 1978 *Magnetic Field Generation in Electrically Conducting Fluids*. Cambridge University Press.

Plunian, F., Marty, P. & Alemany, A. 1999 Kinematic dynamo action in a network of screw motions. Application to the core of a fast breeder reactor. *J. Fluid Mech.* **382**, 137–154.

Sommeria J. & Moreau R. 1982 Why, how, and when, MHD turbulence becomes two-dimensional. *J. Fluid Mech.* **118**, 507–518.

Welch, P. D. 1970 The use of Fast Fourier transform for the estimation of power spectra. *IEEE Trans. Audio. Electroacoust.* **AU-15**, 70–73.

Werkoff, F. & Garnier, J. 1988 Observation of magnetic field generation and distortion in the Phenix liquid-metal fast breeder reactor. In *Liquid Metal Flows: Magnetohydrodynamics and Applications, Proc. 5th Beer-Sheva Seminar on MHD Flows and Turbulence 1987, Jerusalem, Israel* (ed. H. Branover, M. Mond & Y. Unger), vol. 111, pp. 349–360. AIAA.